Flow Around Bluff Body Triangular: Flame Holder

– Assignment 2, May 2023

Tarun Teja, (tarna588)
Abhishek Dhiman, (abhdh352)

LINKÖPINGS UNIVERSITET

Linköping University
Division of Applied Thermodynamics and Fluid Mechanics

1 Introduction

Fluid flow around a stationary body gives rise to the relative velocity between body and fluid. and the flow is referred to as flow over immersed bodies. Depending up on the shape of the immersed body, it is said to be a streamlined or bluff body. In the streamlined body, streamlines travel relatively on the surface of the body and reduce the velocity of the flow due to the viscosity and surface of the body that amplifies the shear stress in the fluid layers near the wall. Whereas, in the case of bluff bodies the flow experiences great blockage and tends to separate near the edges of the body. Flow around some bluff bodies have periodic formation and shedding of circulated flow structures (vortices) in the wake region, also referred to as vortex shedding resulting in flow unsteadiness. Some bluff bodies generate organized vortex-shedding i.e alternating vortices shedding from the top and bottom (in case of cylinder, triangular flame holder etc) part of the body resulting in an unsteady flow, which can also be highly turbulent. Particularly, the bluff bodies are used to enhance the unsteadiness in the flow to promote better mixing and heat and momentum transfer. Turbulent flow around bluff bodies has a wide range of engineering applications (e.g.in electronics cooling, heat exchangers, nuclear reactors, flame holders in jet engine nozzle (afterburners), design of the flow dividers, probes and sensors etc). In the afterburner of some gas turbines, a triangular bluff body is used to reduce the flow velocity to allow for fuel ignition and air mixing in the wake. Triangular cross-section bluff body however being a potential vortex generator is the primary focus of this study aided with existing literature [1] and [2]. The present study mainly discusses the fundamental aspects and terms related to flow parameters, verification and validation of the experimental data from [2].

Section 2 encapsulates the methodology, verification, and investigation of quadrilateral and triangular meshes to explore the strengths and weaknesses of both in capturing vortex shedding. The verification results are compared for average amplitude of velocity in the flame holder wake, lift and drag coefficients of the triangular flame holder, and the Strouhal number describing the oscillating flow. Post verification on Unsteady Reynolds Averaged Navier-stokes (URANS), the validation is conducted for velocities, shear stresses, and turbulent kinetic energy for an unstructured mesh selected based on verification, and the results are presented in Section 3. The results are later compared with the Steady RANS simulation results in order to explore if the simulation costs can be reduced by using steady RANS with acceptable results. The use of $K-\varepsilon$ Realizable (RKE) turbulence model is recommended for verification and validation of the obtained results as the resolution of boundary layers is not the primary focus and the R_e of interest is high in the domain, hence $K-\varepsilon$ turbulence model utilized. In all the above stages maximum Courant No. in the entire domain is kept below 1. Later in the study, the effect of CFL change is explored for Courant No **[1, 2, 3]**. Eventually, the simulation results are post-processed partially in MATLAB and FLUENT results. In sections 4&5, discussion about obtained results and salient features is presented aiding in drawing the conclusion.

2 Methodology

2.1 Model Setup & Boundary conditions

The boundaries and dimensions are set up as shown in Fig. 1 and the boundary conditions are replicated from [1]. The flame holder (triangle shape) and the top and bottom walls are initialized with no-slip conditions. A constant inlet velocity of 16.433 [m/s] is used to achieve the Reynolds Number ($R_{e_H} = 45000$). The outlet is a pressure outlet with gauge pressure = 0 and for normalizing the parameters $H_{ref} = 0.04$ [m] and $U_ref = 17$ [m/s] is used.

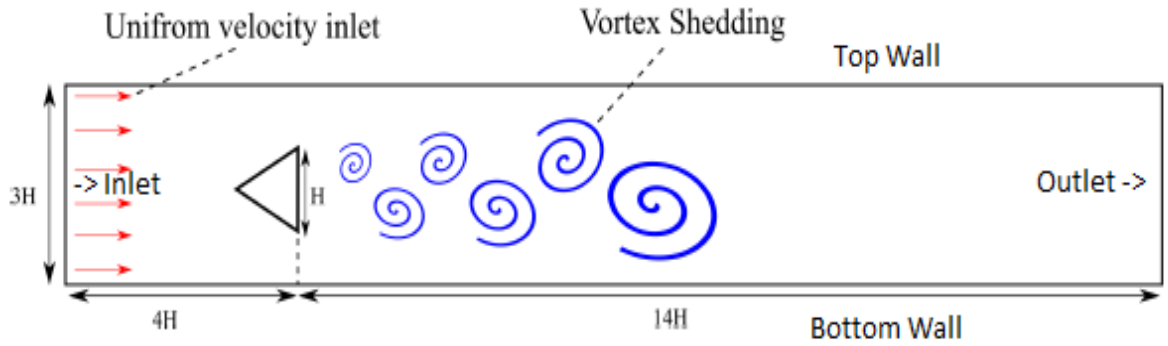

Figure 1: Domain size and boundaries [3]

Pressure-based solver is used for transient behavior as the flow is subsonic and density changes are trivial. The k - ε Realizable model is used with scalable wall function to ensure $y^+ > 11.225$ at the walls. Coupled Algorithm is used for pressure-velocity coupling with 2^{nd} order discretization schemes for pressure and momentum, whereas 1^{st} order for Upwind for Turbulent kinetic energy and dissipation rate. The under-relaxation provided for pressure and momentum is 0.98 and for turbulent variables. The Hybrid initialization is executed and the initial simulations are done for Courant No = 10000 to fast forward the capturing to steady state parameters and resolve instabilities. The time step size is then successively reduced to achieve a maximum CFL of 1 in the entire domain.

2.2 Structured Mesh

The verification of unsteady and transient simulations means that the algorithm/code (Ansys Fluent) is capable of solving a system of highly coupled equations with a valid set of boundary conditions. A sufficiently fine grid is necessary to resolve the gradients and all the other terms of these equations. Hence, the study uses two different types of meshes, namely quadrilateral and triangular. To prevent any discretization error from the mesh, the proposed method for verification by [4] is followed. Commencing with quadrilateral (structured) mesh which offers simplicity and efficiency, it requires less memory compared to unstructured mesh with the same number of elements. The use of structured mesh saves simulation time in many CFD scenarios and complex problems but takes a good amount of time to generate completely structured mesh. Multiple blocks are created in the domain to keep maximum refinement near the triangular flame holder and the wake region behind it. Generally, these multi-blocks are useful in maintaining a structural grid configuration around complex geometries. The details of structured mesh verification are presented in Table. [2].

2.3 Un-Structured Mesh

The unstructured mesh is easier to generate and is ideal for complex geometries, to capture complex mixing flows, and is necessary to incorporate an inflation layer at the wall/surface to capture the various resolved sections boundary layer. On the other hand, consumes a lot of memory and takes a longer time to solve [5]. The details of the unstructured mesh verification are provided in Table. [1] and are discussed in section 2.4. Also, the comparison of structured and unstructured mesh analysis is captured in Table. [4, 5] which aided in the selection process of a suitable mesh for further analysis.

2.4 Mesh Verification

The mesh verification process is followed as described in [4] which serves as the Standard Operating Procedure (SOP) and is accepted by the CFD community. The grid refinement (r in [4]) factor r_{GR} in Table. 2, 1 is kept greater than 1.33 for all meshes and constant as well to 1.6 approx for simpler calculation of grid convergence index (GCI). The amplitude and frequency of certain parameters are monitored for each mesh (structured and unstructured). The parameters include velocity magnitude at a point (2H, H/2) behind the vertical line of the triangular flame holder (called H_v from now on-wards), the lift and drag coefficients are monitored for at H_v, and the Strouhal Number (St) is calculated as $st = \frac{f*V}{L}$, where f = oscillation frequency of velocity, V = velocity amplitude and L = characteristic length (H_v). Once the oscillation in the monitored parameters becomes statistically steady i.e. the mean of oscillation becomes constant, then the mean value of the amplitude is used to estimate the GCI value. The statistical steadiness is identified visually from the monitored plots of each parameter.

The mesh verification study leads to fruitful results with GCI estimated for the statistically stable amplitude of the above-mentioned parameters. The maximum % error of 2.211% for **cd** w.r.t to structured mesh, whereas the un-structured mesh it is 4.855% for Strouhal Number (St) Table. 2 and Table. 1 respectively. Note: The error with cl is significant but the parameter cl itself holds low priority as in practice the flame holder is a fixed component and hence neglected.

The unstructured mesh (M3) is selected for further analysis of transient flow behavior as the GCI values are well within the accepted range ($< 5\%$) [6]. An important observation is that the structured mesh unexpectedly took more computational time to become statistically stable compared to the unstructured mesh for the approx same number of elements. Eventually, the ease of mesh generation and refinement associated with unstructured mesh strengthened the choice of selection.

Unstructured Verification: Mean amplitude of velocity, c_d and c_l

Mesh	**Nodes**	**Elements**	**h**	**r(GR)**	St_{GCI}	$Velocity_{GCI}$	$c_{d_{GCI}}$	$c_{l_{GCI}}$
M1	13360	23824	1.897	-	-	-	-	
M3	34808	66422	1.136	1.67	4.855	0.638	2.561	19.39
M5	87458	170394	0.71	1.602	4.18	0.246	1.29	12.532

Structured Verification: Mean amplitude of velocity, c_d and c_l

Mesh	**Nodes**	**Elements**	**h**	**r(GR)**	St_{GCI}	$Velocity_{GCI}$	$c_{d_{GCI}}$	$c_{l_{GCI}}$
M1	25220	24800	1.859	-	-	-	-	
M3	65855	65125	1.147	1.621	0.149	0.081	1.184	0.11
M5	173770	172600	0.705	1.628	0.953	0.71	2.211	0.005

The CFL study for URANS is performed (not shown in the form of figures) as part of verification. The normalized mean X velocity ($\bar{U}$) at the centerline is used to observe the influence of CFL1, CFL2, and CFL3 i.e. the maximum CFL value in the entire domain which implied that for CFL2 and CFL3 the mean velocity profile deviated significantly compared to CFL1. The peak negative value and the profile downstream of re-circulation in particular showed great

dis-agreement. Hence, for further analysis, the time step is selected to keep CFL1 < 1 in the domain and is monitored along with residuals.

2.5 Statistical Convergence and Sampling Error

Statistical convergence in the time-dependent flow field is associated with two sources of uncertainties i.e. the influence of initial transient and statistical error due to a finite number of samples [7]. The present study followed a procedure to detect and quantify the two sources of errors w.r.t URANS model analogous to the procedure presented in [7] for Scale Resolving Simulation (SRS), however the statistical convergence associated with time averaging applies to URANS as well. The data sampling is performed for c_d, c_l, and mean velocity at three different points in flame holder wake (top, center, and bottom). These five parameters are observed until consistent periodic oscillation is achieved. After this, the procedure [7] is followed in order to estimate the initial transient point and quantify Mean Squared Error (MSE) for sampling error. Post MSE quantification, the data is sampled further to obtain good results for mean velocity profiles, Reynolds shear stress ($u'v'$), and Turbulent kinetic energy (tke).

Step 1: The initial transient identification and removal from the sample data are important in the quantification of statistical convergence of simulation, for which the Marginal Standard Error Rule (MSER) is used [7]. The visual estimation of statistical convergence is prone to human error and varies significantly leading to inconsistency in obtained results. The procedure followed in the present study identifies a truncation point that minimizes the width of the confidence interval about the truncated sample mean, Equation [1, 2] [7]. For URANS (CFL1) the above-mentioned five parameters are monitored. After detecting the transient point, the sampled data till this point is removed and further sampling is done to compensate for this and ensure sufficient sampled data. The sampled data is then used to quantify the sampling error. The sampling error is estimated with an approach based on the direct estimation of sampling error with the utilization of Equation [4] [7] for the quantification of MSE for each flow parameter and presented in Table. 3.

Table 3: Statistical Convergence Sampling Error

Flow Parameter	RANS Sampling Error	URANS Sampling Error
c_d(Flame holder)	2.2397e-15	3.0528e-10
c_l(Flame holder)	2.6104e-19	4.3146e-12
$\bar{U}$(Top point)	1.6025e-11	2.2946e-08
$\bar{U}$(Center point)	3.8396e-14	2.4550e-08
$\bar{U}$(Bottom point)	1.5157e-11	4.7334e-07

2.6 Validation

Post mesh verification, the validation is performed against the experimental results and data of [2]. Once the statistical steadiness is achieved, truncation error removed and sampling error quantified, the sampled data validated for mean velocity profiles, Reynolds stress ($u'v'$), Turbulent kinetic energy (tke) and centerline mean velocity at 5 locations [15, 38, 61, 150, 376] (mm) downstream (wake) of the flame holder. Additionally, the differences between steady (RANS) and unsteady (URANS) simulations are compared and presented in the following section. The obtained results are grid independent and the results from two-dimensional unsteady turbulent flow with a $R_{e_H} = 45000$ are presented.

3 Results

The Strouhal number (St) comparisons (Table. 4 and 5) are important to mention in order to highlight the oscillating flow behavior. The agreement with reference value is good and with an acceptable % error. The error in the case of unstructured mesh is low when compared to structured mesh.

Structured Mesh: Strouhal number (St) comparison

Mesh No	**Mesh1**	**Mesh3**	**Mesh5**
Mesh (St)	0.275	0.276	0.264
% error experiment	9.857	10.588	5.7744
% error simulation	1.72	2.4	2.06
Experiment [2] (St)	0.25	Simulation [2] (St)	0.27

Unstructured Mesh: Strouhal number (St) comparison

Mesh No	**Mesh1**	**Mesh3**	**Mesh5**
Mesh (St)	0.267	0.264	0.266
% error experiment	6.96	5.74	6.55
% error simulation	0.965	2.09	1.345
Experiment [2] (St)	0.25	Simulation [2] (St)	0.27

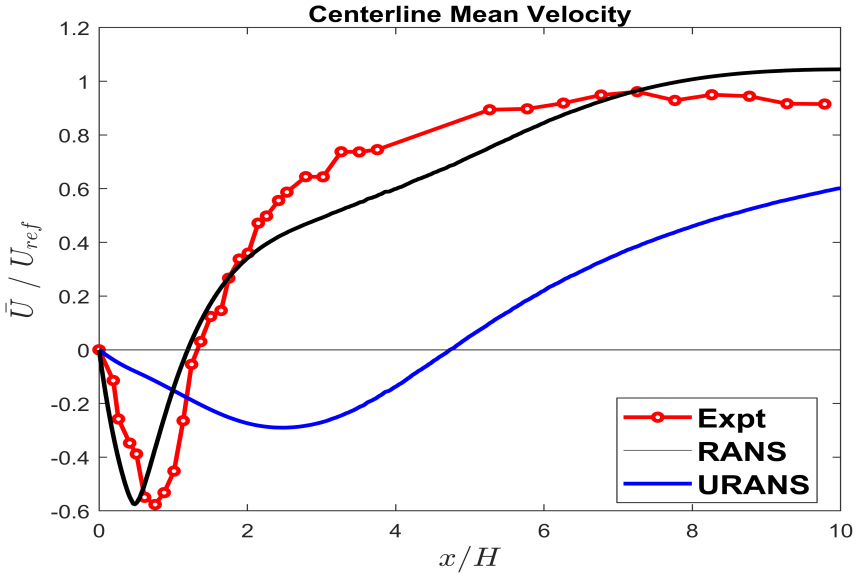

Figure 2: Mean Velocity at center line for URANS & RANS state

The normalized mean X velocity ($\bar{U}$), Fig. [2] shows the mean velocity comparison for both RANS and URANS state along the centerline behind the triangular flame holder. The CFL1

results show good agreement in capturing the overall trend of experimental data. The re-circulation zone (the curves going from negative to the positive y-axis) is underestimated along with the peak value in the re-circulation zone. The downstream profile is well followed. In the case of RANS, the profile captures a re-circulation zone but the overall profile and length of the re-circulation zone are in poor agreement.

For the mean velocity in Fig. [3], the comparison of RANS, and URANS models is made against experimental data. The results of URANS are in good agreement with experimental data at all locations with marginal deviations observed at various peak values. RANS captures the profile and shows satisfactory near-wall agreement but fails to capture the peaks for locations 15mm and 38mm. For downstream locations, RANS progressively over-estimates the profile and fails to show any agreement. The URANS profiles for downstream locations 376 mm significant deviation in peak value and overall profile. Fig. [3e]

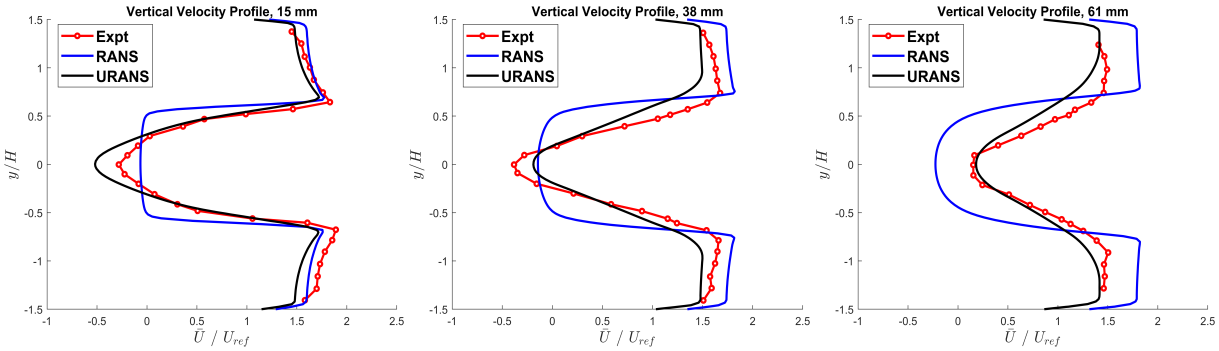

(a) $\bar{U}/U_{bulk}$ **at 15 mm location** **(b)** $\bar{U}/U_{bulk}$ **at 38 mm location** **(c)** $\bar{U}/U_{bulk}$ **at 61 mm location**

(d) $\bar{U}/U_{bulk}$ **at 150 mm location** **(e)** $\bar{U}/U_{bulk}$ **at 376 mm location**

Figure 3: Comparison of mean normalized velocities numerical results and experimental data

The Reynolds shear stress ($u'v'$) results of URANS show great resemblance with the experimental data, Fig. [4]. The number of peaks and peak values is well captured by URANS at all locations but at 15 mm and 61 mm (Fig. 4c) significant discrepancies and under-predictions are present for peaks. Another observation is the near wall agreement i.e. ($-1.5 < y/H < -1$) and ($0.5 < y/H < 1.5$) for URANS is overlapping with experimental data. In the case of RANS, the profile is more or less a straight vertical line at all locations.

The turbulent kinetic energy (tke) shows satisfactory agreement at 15mm, 38 mm, and 61 mm locations with deviations in the prediction of peak values and near peak profile, but the overall profile has a satisfactory resemblance Fig. [5]. At an increased distance, the agreement improves i.e. 150 mm (Fig. 5d) and 376 mm (Fig. 5e). The magnitude of tke gradually increases from 15 mm to 61 mm locations then sharply reduces at 150 mm and further reduces at 376 mm.

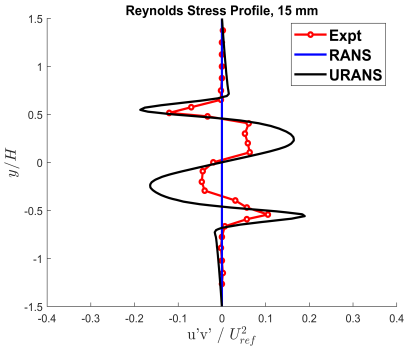

(a) $u'v'/U_{bulk}^2$ at 15 mm location

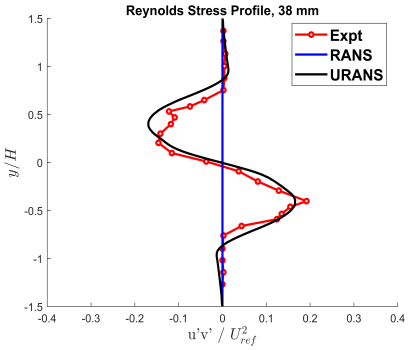

(b) $u'v'/U_{bulk}^2$ at 38 mm location

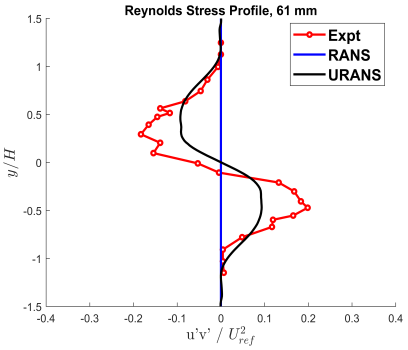

(c) $u'v'/U_{bulk}^2$ at 61 mm location

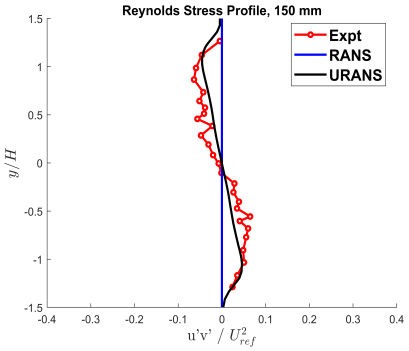

(d) $u'v'/U_{bulk}^2$ at 150 mm location

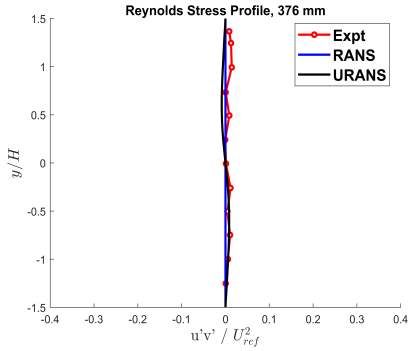

(e) $u'v'/U_{bulk}^2$ at 376 mm location

Figure 4: Comparison of $u'v'/U_{bulk}^2$ between numerical results and experimental data

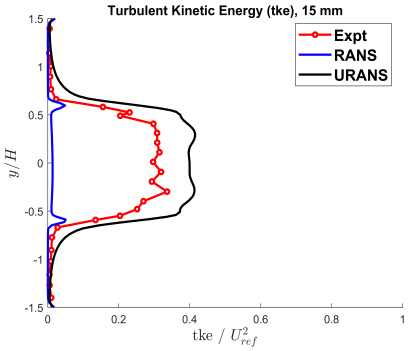

(a) TKE at 15 mm location

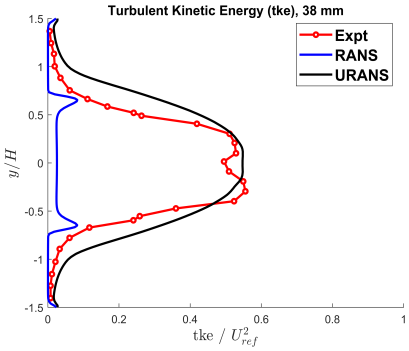

(b) TKE at 38 mm location

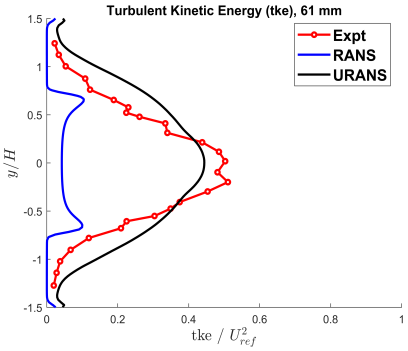

(c) TKE at 61 mm location

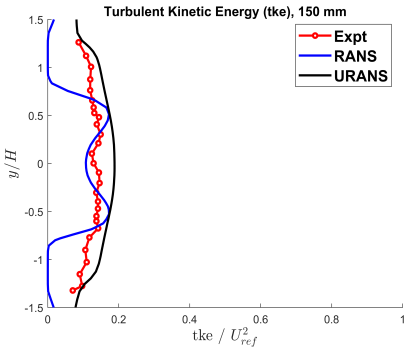

(d) TKE at 150 mm location

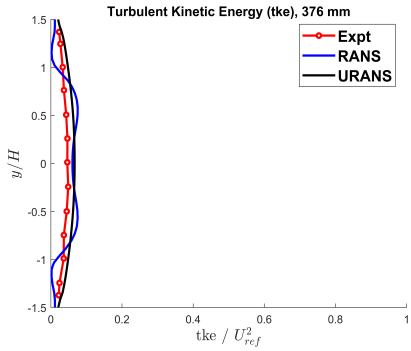

(e) TKE at 376 mm location

Figure 5: Comparison of (tke/U_{bulk}^2) between numerical results and experimental data

4 Discussion

The comparison of St for Mesh3 in Table. 5 is significant in highlighting the achieved flow periodicity i.e. the vortex shedding phenomena. The % error with experiment data [2] is 5.74% which is very close to the acceptable error of 5% [6]. Whereas, upon comparison with simulation results [2] is error 2.09% which is well within an acceptable value.

Fig. 2 showed good agreement with URANS CFL 1. In the case of RANS (k - ε realizable), it is incapable to capture the fluctuating velocity component and hence failed to capture the maximum negative mean velocity and overall profile. The URANS prediction of the maximum negative value slightly upstream is also observed in Johannson [2], along with the under-prediction of mean re-circulation zone length is contrary to Johannson [2] where it is accurately estimated.

The mean velocity negative peak values signify the complex wake region with the formation of re-circulation due to vortex shedding. The peak profile diminishes with downstream movement from 15 mm to 376 mm implying the loss of memory about the wake [2].

The transport of mean momentum by Reynolds shear stress ($u'v'$) dominates the flow in the wake region as seen in Fig. 4a. The presence of local minima and maxima in Fig. 4 are suspected to be correlated to corresponding inflection points at the same location in Fig. 3 which is also highlighted by Johannson [2] as the exchange of momentum is transported by the velocity gradients. The reduced number of minima and maxima as the downstream distance increment signifies the reduction in momentum exchange, especially at locations (150 mm and 376 mm). The vortex shedding phenomenon greatly promotes transversal momentum exchange in the immediate wake region and rapidly decays with velocity further downstream 150 mm and 376 mm [2]. This can be observed from the velocity profiles Fig. [3.

The turbulent kinetic energy (tke) over and under prediction at all the locations indicates that the contribution of fluctuating kinetic energy is satisfactorily captured, implying vortex shedding is stronger (over) or weaker (under) at different locations Fig. 5. But, the observation made in Johannson [2] indicates that the vortex shedding is stronger in experimental flow which would give a larger momentum exchange and faster decay of velocity. The sharp reduction in fluctuation kinetic energy magnitude captured by URANS at 150 mm, and 376 mm is significant compared to upstream locations which are similar to the observation made by Johannson [2]

5 Conclusions

The vortex shedding associated with some bluff bodies gives rise to highly unsteady and complex flow in the wake region of the body, especially at high $R_{e_H} = 45000$ as used in this study. To capture the vortex shedding, k - ε realizable model is used with transient flow physics. The simulation results showed admirable agreement with experimental data. Also, with steady-state RANS the results are fairly good in the estimation of the mean velocity profile at different downstream locations and the center-line. The following conclusions are drawn from the present study.

- The grid refinement in the wake is important to comply with the fine time steps to capture the transient flow and complex vortex shedding phenomena. Hence, the unstructured mesh is suitable for inexpensive transient simulation.

- The un-structured mesh result for Strouhal number (St = 0.264) are in great agreement with experimental (5.74 % error) and simulation (2.09 % error) data.

- The structured mesh of the same number of elements compared to unstructured mesh resulted in more time for mesh generation and simulation and resulted in higher St which is important for flow periodicity.
- The mean velocity and Reynolds shear stress profiles at different downstream locations infer that vortex shedding promotes the momentum exchange.
- The number of local maxima and minima in $\bar{U}$ and $u'v'$ profiles signifies better momentum mixing region in the wake i.e. up to 61 mm downstream.
- The CFL number must be kept $<= 1$ to obtain good results in unsteady and complex flow physics.
- The k - ε realizable is with high R_{e_H} greatly captured salient features of the complex unsteady flow.

References

[1] Christian Hasse MW Volker Sohm, Durst B. Hybrid URANS/LES Turbulence Simulation of Vortex Shedding Behind a Triangular Flameholder. 2008.

[2] Stefan H Johansson LD, Olsson E. Numerical Simulation of Vortex Shedding Past Triangular Cylinders At High Reynolds Number Using A k-ε Turbulence Model. 1993.

[3] GËardhagen SFR. Flow Around Triangular Bluff Body TMMV07 Assignment 2. 2023.

[4] et al IBC. Procedure for Estimation and Reporting of Uncertainty Due to Discretization in CFD Applications. 2008.

[5] Meshing in FEA: Structured vs Unstructured meshes;. Available from: `https://onscale.com/meshing-in-fea-structured-vs-unstructured-meshes/`.

[6] Fred Stern HWC Robert V Wilson, Paterson EG. VERIFICATION AND VALIDATION OF CFD SIMULATIONS. 1999.

[7] Michael Bergmann GAEK Christian Morsbach. Statistical Error Estimation Methods for Engineering-Relevant Quantities From Scale-Resolving Simulations. 2021.